

Multidirectional UV Lithography for Complex 3-D MEMS Structures

Yong-Kyu Yoon, *Member, IEEE*, Jung-Hwan Park, and Mark G. Allen, *Senior Member, IEEE*

Abstract—Various three-dimensionally (3-D) complex MEMS structures are fabricated using multidirectional ultraviolet (UV) lithography, which includes reverse-side exposure through a UV-transparent substrate, inclined exposure with or without simultaneous substrate rotation, and the combination of these processes. A reverse-side exposure scheme through UV-transparent substrates (e.g., glass, sapphire, or quartz) has been exploited for implementing high-aspect-ratio structures (greater than 20:1), repeatable self-alignment photoresist patterning with subsequent metallization on a BST/sapphire substrate, and unconventional patterning using substrate optics such as proximity patterning or integrated lens techniques. Inclined exposure has been applied to a SU-8 substrate with differing inclination angles and incidence directions. The refractive index of SU-8 is experimentally determined to be 1.68 by means of test structures fabricated using this approach. Implemented structures using the inclined exposure include vertical screen structures, inclined tubes, and conical shape structures. Dynamic mode operation, in which the substrate is continuously rotated and tilted during exposure is also discussed. Examples of achievable 3-D structures using dynamic mode operation are presented. [1581]

Index Terms—Inclined exposure, multidirectional ultraviolet (UV) lithography, reverse-side exposure, rotational exposure, SU-8.

I. INTRODUCTION

ULTRAVIOLET (UV) lithography is widely used for three-dimensional (3-D) MEMS structure fabrication since the equipment utilized in fabrication is relatively inexpensive compared to X-ray or laser systems [1]–[3]. However, most conventional UV lithography systems have been designed for 2-D patterning; i.e., the relative position between light source and substrate is prefixed, and, therefore, fabricated 3-D sidewalls are normal to the substrate as shown in Fig. 1(a). Given these constraints, early work in UV-based 3-D fabrication research focused almost exclusively on the implementation of high-aspect-ratio structures “extruded” normal to the substrate surface.

The photopatternable, negative-tone epoxy resin SU-8 was introduced to the MEMS community in the mid-1990s. Very high-aspect-ratio microstructures have been implemented from SU-8 photoresist (PR) using UV or near-UV light sources [4]–[7]. For patterning thick, high-aspect-ratio structures, good physical contact between photomask and photoresist is necessary, and a hard contact or vacuum contact mode is usually used

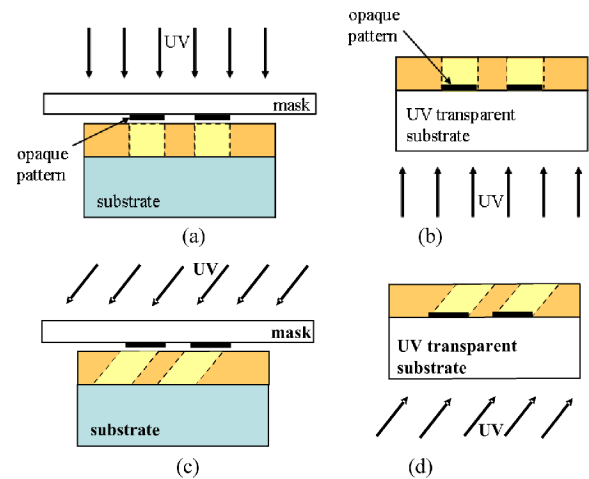


Fig. 1. Multidirectional UV exposure scheme. (a) Normal front-side exposure. (b) Normal reverse-side exposure through a transparent substrate. (c) Inclined front-side exposure. (d) Inclined reverse-side exposure through a transparent substrate.

rather than proximity mode. However, this places a constraint of planarity on the upper surface of the resin. Alternatively, when an optically UV transparent material (e.g., glass, sapphire, or quartz) is employed as a substrate, reverse-side (or back-side) UV exposure through the substrate in which the substrate bears a prepatterned photomask layer, can be utilized to obtain sharp photo patterns resulting from the intimate contact between the photomask/substrate and the resin. A schematic viewgraph of this reverse-side exposure approach is shown in Fig. 1(b) [8]–[10].

To fabricate more complex 3-D structures, an inclined light exposure scheme has been employed in X-ray lithography [11], [12] and UV lithography [13], where the light has an arbitrary incident angle between 0° and 90° from the vertical line of the photomask or substrate plane. The inclined UV exposure can be performed in a front-side scheme or a reverse-side scheme as shown in Fig. 1(c) and (d), respectively, for both opaque and transparent substrates. Recently, the inclined UV exposure scheme has also been applied to SU-8 patterning to produce high-aspect-ratio inclined structures and complex microfluidic structures such as a filter, a mixer, and a dispenser [14]–[22]. Inclined exposure also has been applied to a substrate in a liquid environment to achieve more angled structures for optical applications [23], [24].

In this paper, multidirectional UV exposure schemes are discussed, which includes the reverse-side exposure and the inclined exposure approaches. The first part of this paper discusses the normal-incidence, reverse-side exposure scheme in

Manuscript received April 22, 2005; revised February 8, 2006. Subject Editor C. Liu.

The authors are with the School of Electrical and Computer Engineering, Georgia Institute of Technology, Atlanta, GA 30332 USA (e-mail: yongkyu.yoon@ece.gatech.edu).

Color versions of Figs. 1, 2, 4, 5, 6, 7, 8, 12, 15, 16, 17, and Table II are available online at <http://ieeexplore.ieee.org>.

Digital Object Identifier 10.1109/JMEMS.2006.879669

three application areas: implementing high-aspect-ratio structures (greater than 20:1); repeatable self-alignment photoresist patterning with subsequent metallization on a BST/sapphire substrate; and unconventional patterning using substrate optics such as proximity patterning or integrated lens techniques. The second part of this paper discusses the inclined exposure approach. The inclined structure is described from the point of view of inclined angle and incident direction. The optical characteristics of SU-8 and their impact on inclined structures are discussed. To illustrate the process, various structures fabricated from single and multiple inclined exposure, both with and without substrate rotation are demonstrated, including vertical screen structures, inclined tubes, and conical shape structures.

II. REVERSE-SIDE EXPOSURE

MEMS or microelectronic devices can utilize various materials as substrates. Some materials such as Si, GaAs, alumina, and metal, are opaque to the UV light source, while others such as glass, quartz, and sapphire, are transparent to it. When optically transparent materials are employed as substrates, additional flexibility is achievable in photolithographic patterning. For example, appropriate optical doses can be applied not only from the front-(upper-) side, but also from the reverse- (back-) side. In the case of the reverse-side exposure, the photomask (usually a chromium layer) can be prepatterned before the photoresist (PR) layer is applied. In this section, useful applications of the reverse-side exposure through transparent substrates are discussed in three subsections: fabrication of a high-aspect-ratio structure, a self-aligned microelectrode fabrication scheme, and the usage of substrate optics to produce high-aspect-ratio, tapered structures.

A. High-Aspect-Ratio Patterning

The fabrication sequence for the reverse-side exposure, high-aspect-ratio SU-8 patterns is shown in Fig. 2(a). A thin masking metal layer (usually 200 nm of Cr) is deposited and patterned on the transparent glass substrate. Thick SU-8 is applied on the substrate, followed by UV exposure through the substrate mask layer [Fig. 2(a), left]. In practice, the sample is turned over and placed under a regular UV system with light incident from the top. A high-aspect-ratio structure is obtained after development [Fig. 2(a), right]. The mask layer can either be removed or allowed to remain depending on the requirements of the subsequent steps. Fig. 2(b) shows high-aspect-ratio column structures fabricated with the good contact resulting from reverse-side exposure. Aspect ratio (height to diameter) is approximately 13:1.

This approach provides several advantageous features compared to the front-side exposure for high-aspect-ratio fabrication. First, a secure contact between the photo mask layer and the polymer layer can be provided regardless of surface roughness or edge-bead formation during or after a polymer coating step, thereby allowing a sharp pattern to be obtained. (This is true because in contact photolithography, poor contact causes the diffraction of light at the edge of an opaque feature in the mask, potentially resulting in blurred or diffused pattern edges.)

Using the reverse-side exposure scheme, usually more optical dose is absorbed in the bottom portion of the column compared to the top portion, resulting in a structure with larger mechanical

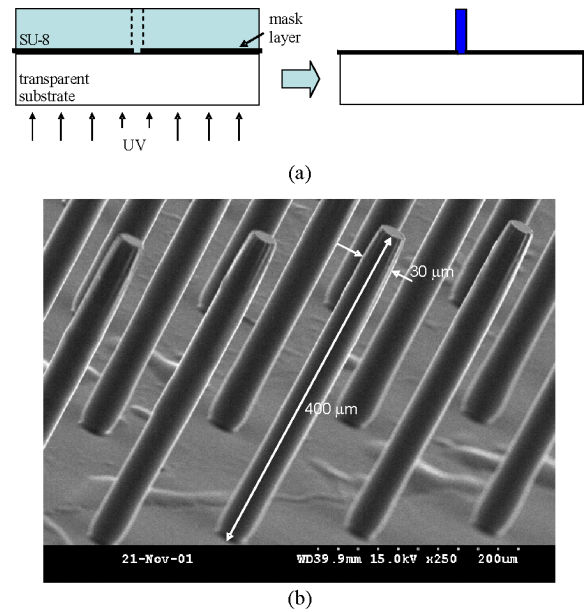


Fig. 2. High-aspect-ratio column structure with reverse-side exposure. (a) Fabrication schematics. (b) Fabricated structure.

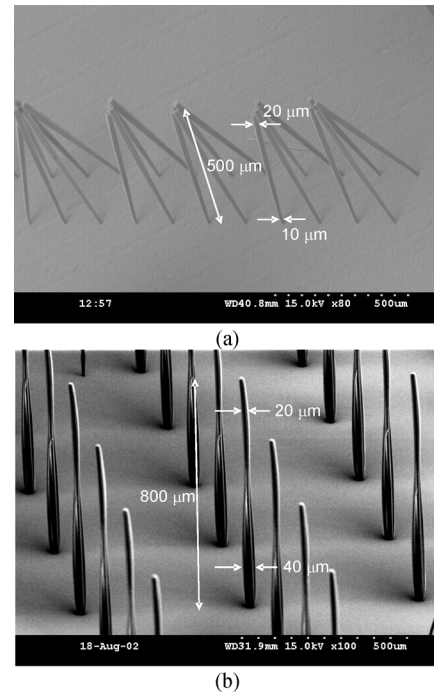


Fig. 3. Fabricated high-aspect-ratio tapered column structures using (a) front-side exposure and (b) reverse-side exposure.

strength in the lower portion of the column. Often this causes a column structure gradually tapered down to the top compared to a column structure gradually tapered down to the bottom from a more typical front-side exposure scheme. Fig. 3 shows fabricated tall column structures using (a) regular front-side exposure and (b) reverse-side exposure in which both photomask patterns are circular and have diameters of 20 μm. Fig. 3(a) shows the diameter of the top portion of the column is 20 μm while that of the lower portion is 10 μm, thinner due to lack of optical dose, where the height is 500 μm. The structures are

mechanically weak in the lower portion, often leaning over toward others in their group during the drying step due to solvent surface tension. In contrast, the columns fabricated from the reverse-side exposure are nicely standing up to $800\text{ }\mu\text{m}$ tall as shown in Fig. 3(b). However, this particular sample shows a diameter of the bottom portion larger (i.e., $40\text{ }\mu\text{m}$) than the photomask pattern size ($20\text{ }\mu\text{m}$). This phenomenon could be attributable in part to light diffraction in the proximity of the photomask pattern exacerbated by the large exposure doses for these thick films as well as lateral thermal diffusion of the photoacidic reaction products from the exposed area during overexposure. This bottom widening effect is gradually reduced as the ray trace moves to the upper portion, terminating in the designed diameter of $20\text{ }\mu\text{m}$. As a result, mechanically strong and slightly tapered column structures are obtained from the reverse-side exposure and an unoptimized aspect ratio (conservatively defined as a ratio of height to width in the thickest portion) of 20:1 has been achieved.

B. Self-Alignment Scheme

Narrowly spaced thick electrodes are fabricated using a self-aligned multiple lift-off process with reverse-side exposure through a UV transparent substrate. In general, a photoresist mold for a successful lift-off process should be much thicker than the ultimate conductor which is patterned by the lift-off process. When it is necessary that two thick conductors with a very narrow gap between them be fabricated using a lift-off process (e.g., in the case that metal etching might harm an acid-sensitive underlying layer), a high-aspect-ratio polymer mold is required, thereby increasing the process difficulty. It is potentially possible to reduce the thickness of resist required by performing sequential deposition and lift-off steps, thereby building up the required metal thickness in multiple layers; however, the disadvantage of this approach is that multiple alignments, with the associated expense and tolerance errors, would be required. The reverse-side exposure approach can eliminate the need for repeated alignments, while simultaneously preserving the possibility for multilayer film deposition.

Fig. 4(a) shows an example of this fabrication process. Metal patterning ($1\text{ }\mu\text{m}$ thick) is obtained using a standard lift-off process with a relatively thin PR mold [Fig. 4(a)-1]. This metal pattern will then act as an optical mask for reverse-side lithography. Since the goal of this process is metal patterning, as opposed to the fabrication of epoxy structures, a thick, negative tone photoresist (NR9-8000, Futurrex, Inc.) is used as the PR layer, which is easily removed in acetone. The PR is coated and the reverse-side exposure is performed using the previous metal layer as a photo mask in a self-aligned fashion [see Fig. 4(a)-2]. In addition, the resultant mold adheres securely to the substrate after development since the contact area between the mold and the substrate increases as much as the side wall of the first metal layer [see Fig. 4(a)-3]. A second lift-off is performed to obtain even thicker electrodes [see Fig. 4(a)-4]. Additional metal layers can be added by repeating steps 2–4 if necessary. Narrowly spaced thick conductors with a gap of $1.2\text{ }\mu\text{m}$ and a thickness of $2.2\text{ }\mu\text{m}$, which are used for a ferroelectric gap capacitor with low conductor loss, are successfully fabricated as shown in

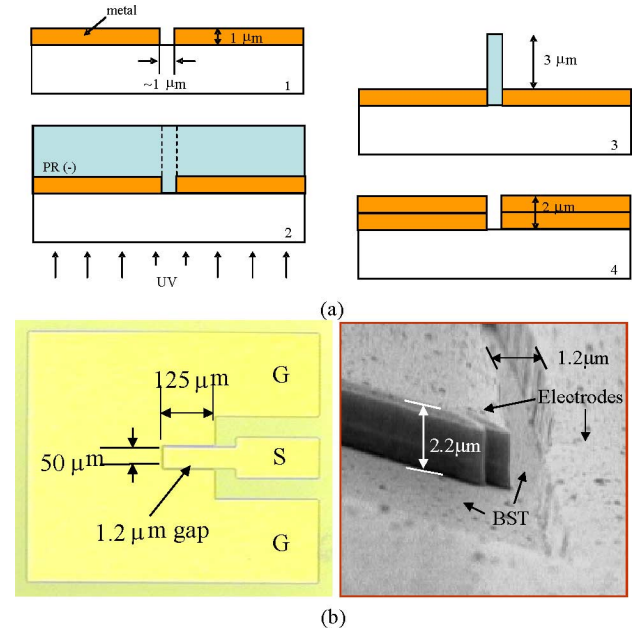


Fig. 4. Narrowly spaced thick electrodes using repeated multiple lift-off processes with self-alignment reverse-side exposure. (a) Fabrication process. (b) Fabricated single digit RF gap capacitor with $1.2\text{ }\mu\text{m}$ gap and $300\text{ }\mu\text{m}$ coupling length – top view (left) and angled SEM view (right) (final metal thickness is $2.2\text{ }\mu\text{m}$), where G and S stand for a ground and signal pad, respectively.

Fig. 4(b). The beneficial effects of the increased electrode thickness on Q-factor and RF performance of these capacitors in the RF frequency range are detailed in [8].

C. Usage of Substrate Optics

Reverse-side exposure through a modified substrate photomask or a micromachined substrate can produce various unusual patterns. When polymer is coated on the metal side (i.e., the side of the photomask bearing the Cr layer or patterned Cr layer), the optical ray trace from reverse-side UV exposure is different from when polymer is coated on the other (glass) side of the photomask. Fig. 5 shows an example of ray trace schematics and fabricated SU-8 structures for a ring shape pattern array. When SU-8 is coated on the metal side, the resultant structure shows a vertical tube—a vertical extrusion of the original ring shape [see Fig. 5(a)], while when SU-8 is coated on the glass side, the resultant pattern shows a mountain shape with a crater on the top [see Fig. 5(b)]. In the latter case, the incident light first meets the mask pattern and is diffracted at the edge of the opaque mask pattern. This light has a large lateral deviation from the originally incident light after its passage through the 1.5 mm thick glass substrate. The light is then further refracted at the interface of glass and SU-8 due to the difference of their refractive indices. A ring pattern of an inner diameter of $100\text{ }\mu\text{m}$ and an outer diameter of $200\text{ }\mu\text{m}$ produces a resultant mountain shape with an inner diameter of the crater, an outer diameter of the crater, a bottom diameter, and a height of $88\text{ }\mu\text{m}$, $140\text{ }\mu\text{m}$, $458\text{ }\mu\text{m}$, and $700\text{ }\mu\text{m}$, respectively as shown in Fig. 5(b).

Another example of reverse-side exposure using substrate optics is shown in Fig. 6. A substrate with an isotropically etched concave shape results in an integrated lens functionality when

TABLE I
TAPERED STRUCTURES FABRICATED USING DIFFERENT SCHEMES

| | Bottom width (d_b) [μm] | Top width (d_t) [μm] | Height (h) [μm] | Tapering ratio ($T = (d_b - d_t)/h$) |
|-----------|--|---------------------------------------|----------------------------------|--|
| Figure 3b | 40 | 20 | 800 | 1/40 |
| Figure 5a | 458 | 140 | 700 | 1/2.2 |
| Figure 6b | 106 | 3 | 1197 | 1/12 |

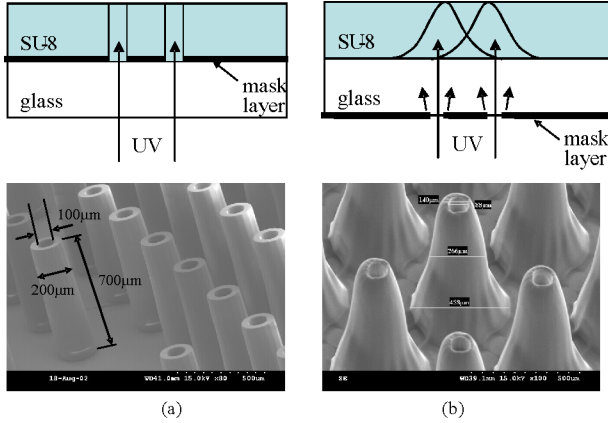


Fig. 5. Reverse-side exposure with the resist layer on differing sides of the substrate. (a) SU-8 on the metal side – schematic (upper) and resultant structure (lower). (b) SU-8 placed on the glass side – schematic (upper) and resultant structure (lower).

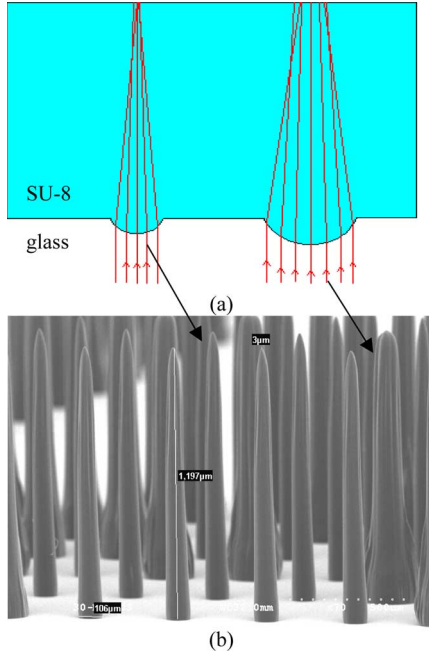


Fig. 6. High-aspect-ratio tapered structure using integrated lens technique. (a) Ray trace simulation for the integrated lens. (b) Fabricated structure.

the concave regions are filled with a material with a different refractive index than the substrate. High-aspect-ratio tapered structures have been fabricated using this modified substrate effect and a 2-D ray trace software (IME Software, Inc.) has been used for the optical simulation as shown in Fig. 6(a) [25]. In Fig. 6(b), a slender conical needle is shown. It has a bottom diameter, a tip radius of curvature, and a height of 106 μm , 3 μm , and 1197 μm , respectively. In contrast to the column structure

fabricated from reverse-side exposure through a planar (i.e., no lens) substrate as shown in Fig. 3(b), the structure shows a significant change in diameter from 106 μm at the bottom to 3 μm at the top due to the integrated convex lens effect. This approach may also have a strengthening effect on the produced microstructures. The focusing effect of the lens causes the optical dose to be increased at any elevation between the substrate and the lens focal point when compared to a planar substrate exposure for the same lamp intensity and exposure time. Depending on the material used, this can result in enhanced crosslinking and therefore mechanical strength of the structure at the otherwise fragile tip. The height of the tapered structure is dependent upon the focal length of the integrated lens as well as the thickness of the SU-8 layer. If the focal length of the integrated lens is smaller than the thickness of SU-8, the height of the structure is determined by the focal length, producing a sharp tip. Such structures have been demonstrated as useful in microneedle applications [25]. Otherwise, the structure height is determined by the thickness of the SU-8, producing a blunt, truncated tapered structure [see Fig. 6(b)].

The tapering ratio T can be defined as the ratio of the difference between the diameter of the top portion d_t and the diameter of the bottom portion d_b to the height h ($T = (d_b - d_t)/h$). Tapering ratios both for integrated lens techniques as well as the other techniques discussed in this section are calculated and summarized in Table I. The tapering ratios for Figs. 3(b), 5(b), and 6(b) are 1/40, 1/2.2, and 1/12, respectively.

III. INCLINED EXPOSURE

In this section, inclined UV exposure schemes are discussed. UV-opaque substrates allow only front-side inclined exposure while UV-transparent substrates allow both front-side and reverse-side inclined exposure. However, for inclined exposures, when the resist has a refractive index that differs from the medium surrounding it, the effect of index differences must be considered. When UV light is incident to a polymeric slab from the air with an incident angle θ_i , the light is refracted at the interface of the two materials. This effect can be illustrated by further use of ray-tracing. Fig. 7 shows the refracted light in the polymeric slab through a clear window of a dark field photomask and is described using a spherical coordinate system (r, θ_r, ϕ) , where r is the nominal length of the ray in the polymeric slab, θ_r the refraction angle from the z axis (the *latitudinal angle*), and ϕ the angle from the x axis in the x - y plane (the *longitudinal angle*).

Inclined exposure can be achieved by tilting or moving the UV source while keeping the substrate fixed; or by placing the substrate on a tilting or rotating stage relative to a fixed UV source. The latter approach allows the usage of standard UV

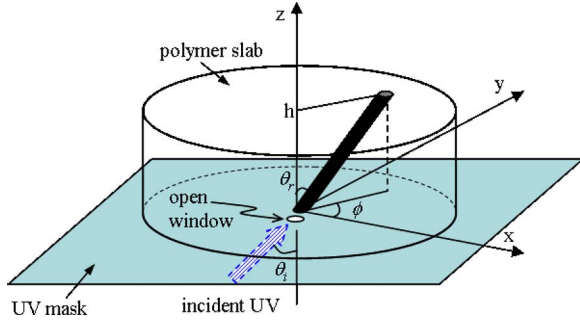


Fig. 7. Coordinate system for inclined UV exposure.

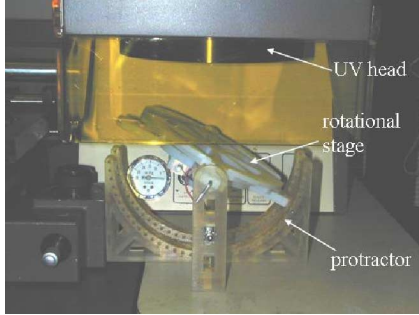


Fig. 8. Substrate/mask holder with tilting and rotational functionality.

aligner equipment with minimal modification. A movable substrate/mask holder suitable for this purpose is shown in Fig. 8, where the substrate holder can be tilted from 0° to $\pm 90^\circ$ and also be continuously rotated in a tilted position.

Inclined exposure experiments include 1) incidence with multiple latitudinal angles, 2) incidence of multiple longitudinal angles, and 3) incidence with continuously varying longitudinal angle (in a rotational mode).

A. Incidence With Multiple Latitudinal Angles

($\phi = \text{fixed}$, $\theta_i = \text{various}$)

Multiple latitudinal UV incidence with a fixed longitudinal angle has been applied to an SU-8 slab through a clear window in a dark field photomask (usually the substrate is glass or quartz). The incident UV light runs across two interfaces: one between air and glass, the other between glass and SU-8. Since the refractive indices of SU-8, glass, and air are different, the incident light is refracted at each interface. The relationship between refractive indices and refractive angles is given as (1) by Snell's law for the three-layer system as shown in Fig. 9

$$n_1 \sin \theta_1 = n_2 \sin \theta_2 = n_3 \sin \theta_3 \quad (1)$$

where n_1 , n_2 , and n_3 are the refractive indices of air, glass, and SU-8, respectively, and θ_1 , θ_2 , and θ_3 the incident angle in air, the refracted angle in glass, and the refracted angle in SU-8, respectively. The refracted angle in SU-8 can be obtained by (2) if the refractive index of air n_1 , the refractive index of SU-8 n_3 , and the incident angle θ_1 are known.

$$\theta_3 = \sin^{-1} \left(\frac{n_1}{n_3} \sin \theta_1 \right). \quad (2)$$

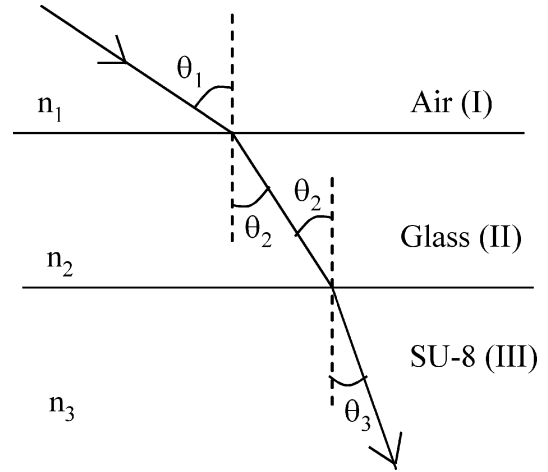
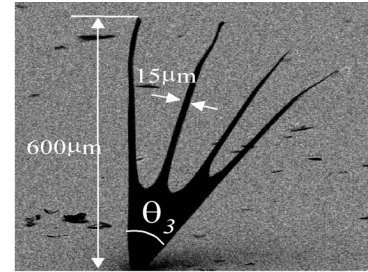
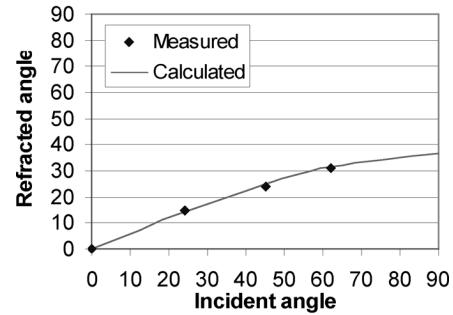


Fig. 9. Light refracted at the interfaces due to different refractive indices of materials.



(a)



(b)

Fig. 10. Angular dependence of exposure. (a) SU-8 pattern multiply exposed with multiple latitudinal incident angles. (b) Refracted angle versus incident angle.

Fig. 10(a) shows a fabricated multi-finger SU-8 structure with a height of $600 \mu\text{m}$, resulting from multiple latitudinal UV incidence through a $15 \mu\text{m}$ diameter clear window in a dark field photomask by reverse-side UV (i-line, 365 nm) exposure. The measured refracted angles are 0° , 15° , 24° , and 31° for the incident angles of 0° , 24° , 45° , and 62° , respectively, as shown in Fig. 10(b). Correlating (1) and the measurement data gives a refractive index of approximately 1.68 for SU-8, which is in good agreement with literature values [26].

Fig. 11 shows fabricated inclined solid columns, hollow columns, and channels. The inclined solid column has a diameter of $50 \mu\text{m}$. The circular hollow column has an inner and outer diameter of $100 \mu\text{m}$ and $200 \mu\text{m}$ while the rectangular hollow column has an inner and outer rectangle of $140 \mu\text{m}$ by

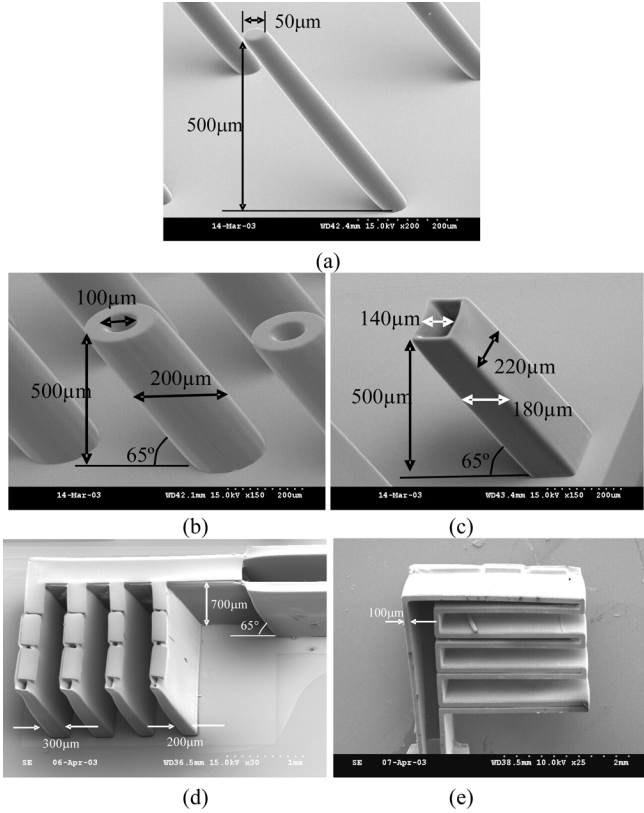


Fig. 11. Fabricated SU-8 structures with single inclined exposure. (a) Solid column array. (b) Circular hollow column array. (c) Rectangular column. (d) Channel network (top-side overlook view). (e) Channel network after separating it from the substrate (reverse-side overlook view).

180 μm and 180 μm by 220 μm , respectively. The inclined columns and tubes are 500 μm tall and are inclined at an angle of 25° from the vertical. The inclined channel network has a height of 700 μm and an inclined angle of 25° . Fluid flows through the in-plane channels and exits through the openings on the top surface, where the channel cap has been formed using shallow exposure and oven baking [27], [28] without blocking the channels as shown in Fig. 11(d). These inclined columns and channels can be combined with vertical laser ablation to have side holes for a microdispenser application [15], [29].

B. Incidence With Multiple Longitudinal Angles ($\phi = \text{various}$, $\theta_i = \text{fixed}$)

Two inclined UV incidences with 180° difference in the longitudinal angle (i.e., $\phi = 0^\circ, 180^\circ$) are used to form a screen filter structure. Fig. 12 shows the fabrication process. A photomask with a series of open windows is placed on an SU-8 coated substrate [see Fig. 12(a)]. The substrate is tilted from the horizontal plane with an angle θ_i where $\phi = 0^\circ$, and UV exposed from the top, where the tilted angle (or the incident angle) is equal to the latitudinal angle θ_i of the coordinate system in Fig. 7 [see Fig. 12(b)]. The substrate is tilted from the opposite longitudinal angle ($\phi = 180^\circ$) with a tilted angle θ_i , and UV exposed from the top [see Fig. 12(c)]. After post exposure bake, the sample is developed to complete a vertical screen structure with diamond shape meshes [see Fig. 12(d)].

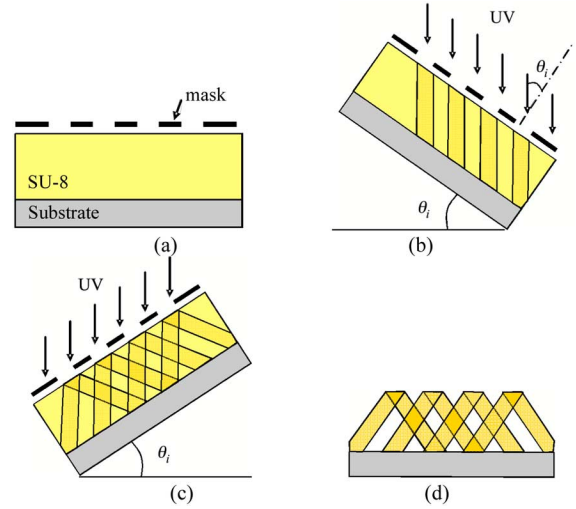


Fig. 12. Fabrication process for a vertical screen structure using multiple inclined exposure.

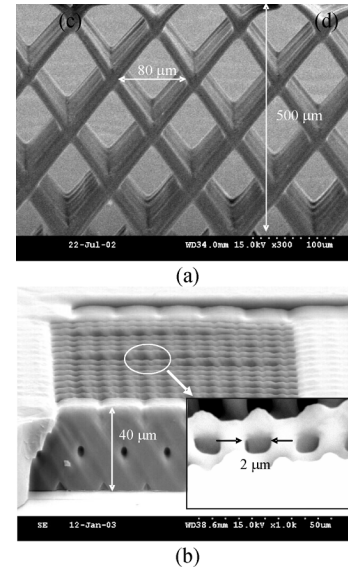


Fig. 13. Vertical screen filter structures with different mesh sizes. (a) Large mesh with a horizontal diagonal of 80 μm . (b) Small mesh with a horizontal diagonal of 2 μm .

The achievable mesh size and shape are determined by the space and pitch of the open windows and the tilted angle. Screen structures with various mesh sizes are fabricated using differing sizes of windows and spaces as shown in Fig. 13. One is fabricated using a photomask of a clear window array with a width of 20 μm and a space of 80 μm . The height of the screen is 500 μm [see Fig. 13(a)]. The other is with both a width and a space of 2 μm over 40 μm tall structures [see Fig. 13(b)]. Both structures are fabricated using reverse-side inclined exposure for a secure mask-to-polymer contact. An aspect ratio (defined as the ratio of the horizontal mesh width to the total screen height) of 20:1 has been achieved with the small mesh structure. An additional advantage of this vertical screen structure formation is that differing meshed structures as well as microfluidic channels can be simultaneously fabricated in the same inclined exposure steps. Fig. 14 shows integrated vertical screen microfluidic filters with

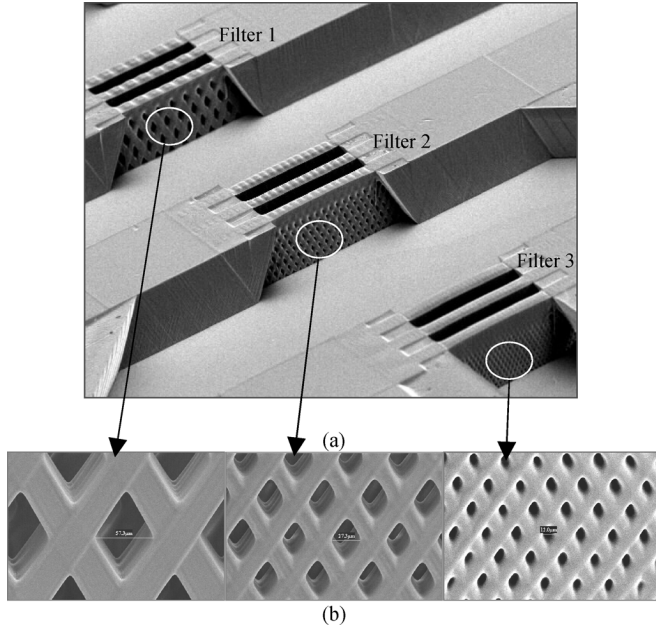


Fig. 14. SEM of (a) Simultaneously fabricated three integrated filters and channels with different mesh sizes and (b) Different mesh sizes: (left) Filter 1; (middle) Filter 2; (right) Filter 3. Horizontal diagonal has been measured to be $57.3 \mu\text{m}$, $27.3 \mu\text{m}$, and $10.0 \mu\text{m}$, respectively.

different mesh sizes (57 , 27 , and $10 \mu\text{m}$) and channels, where the channel height is $390 \mu\text{m}$ [14]. This screen filter structures can be used for various microfluidic filters and mixers [14], [18]. Also, applications can be extended to millimeter wave or higher frequency waveguides, filters, mixers, photonic bandgap (PBG) with appropriate metallization. For high frequency conductor implementation, a polymer-core conductor approach [27], [28] can be utilized. RF passive components and various millimeter wave antennas such as a monopole antenna, an Yagi-Uda antenna, and a patch antenna based on this technology have been successfully demonstrated [30]–[32].

Four inclined UV incidences with 90° difference from each other in the longitudinal angle (i.e., $\phi = 45^\circ$, 135° , 225° , and 315°) are performed as shown in Fig. 15(a). Fig. 15(b), (d) and (c), (e) show fabricated structures with a single rectangle clear window and a multi rectangle clear window array, respectively. A front-side exposure scheme is used for both cases. Fabricated structures manifest proximity exposure with a gap g between the photomask and the substrate as shown in Fig. 15(f), (g). In this structure, the gap g has resulted from warpage of the printed wiring board (PWB) substrate that was utilized. However, this same effect can be achieved on flat substrates by use of spacers of known thickness to control the proximity effect.

C. Continuously Varying Longitudinal Angle ($\phi = 0^\circ \sim 360^\circ$, $\theta_i = \text{various}$)

In the previous section, static mode operation is demonstrated, in which the reflected latitudinal angle θ_r and the longitudinal angle ϕ are fixed during each UV exposure. It is also possible to consider dynamic mode operation, in which both the latitudinal angle θ_r and the longitudinal angle ϕ can vary during exposure. Using the coordinate system in Fig. 7,

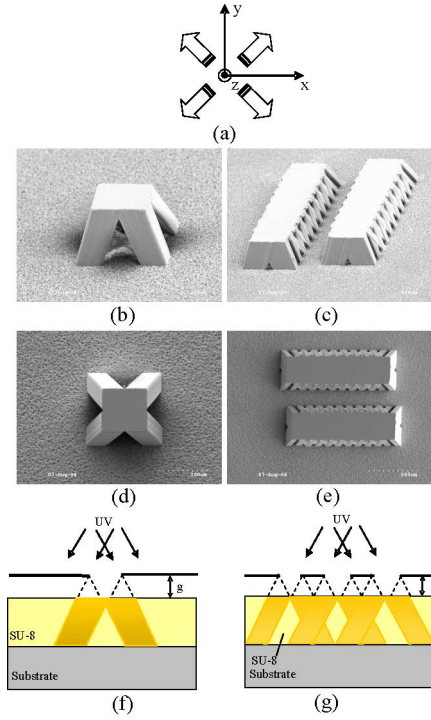


Fig. 15. Fabricated structures from four directional UV incidence with 90° difference each other. (a) Longitudinal angle of 45° , 135° , 225° , and 315° . (b) Structure from a single clear window (oblique view). (c) Structure from a clear window array (oblique view). (d) Top view of structure b. (e) Top view of structure c. (f) and (g) Schematics of proximity exposure with a gap g between the photomask and the substrate for structures b and c, respectively.

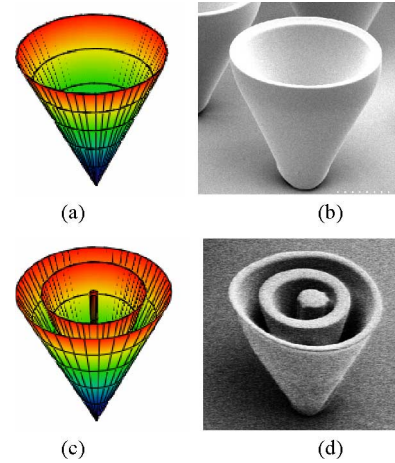


Fig. 16. Horn structures fabricated using continuously rotational inclined UV exposure. (a) Simulated. (b) Fabricated single horn. (c) Simulated. (d) Fabricated multishelled horn.

(x, y, z) of the inclined ray trace through the open window can be described as follows:


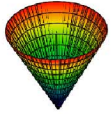
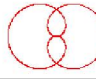


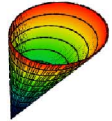
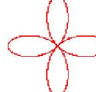
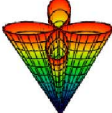


$$x = r \sin \theta_r \cos \phi = z \frac{\sin \theta_r}{\cos \theta_r} \cos \phi = z \tan \theta_r \cos \phi \quad (3)$$

$$y = z \tan \theta_r \sin \phi \quad (4)$$

$$z = z \quad (5)$$

where θ_r and ϕ are functions of time. As an example, with a latitudinal angle θ_r fixed and a longitudinal angle ϕ varying in an

TABLE II
INCLINED EXPOSURE PATTERNS IN DYNAMIC MODES WITH A CONTINUOUSLY VARYING ROTATIONAL AND
TILTING SUBSTRATE (THE ROTATIONAL FREQUENCY ω_1 AND THE TILTING FREQUENCY ω_2
ARE SYNCHRONIZED)

| Tilting frequency (ω_2) | Distance from z-axis at $z = h$ during exposure | 2-D projection of resultant 3-D shape | Peak angles (ϕ) | Null positions (ϕ) | 3-D schematic |
|----------------------------------|---|---|-------------------------|---------------------------------|--|
| 0 | $h \tan \theta_{r0}$ | Circle  | $0-2\pi$ | NA |  |
| $\omega_1/2$ | $h \tan(\theta_{r0} \cos(\omega_1/2)t)$ | Double Cardiac shape  | 0 | $\pi, 3\pi$ |  |
| ω_1 | $h \tan(\theta_{r0} \cos \omega_1 t)$ | A single lobe  | 0 | π |  |
| $2\omega_1$ | $h \tan(\theta_{r0} \cos 2\omega_1 t)$ | 4 lobes  | $0, \pi/2, \pi, 3\pi/2$ | $\pi/4, 3\pi/4, 5\pi/4, 7\pi/4$ |  |
| $3\omega_1$ | $h \tan(\theta_{r0} \cos 3\omega_1 t)$ | 3 lobes  | $0, 2\pi/3, 4\pi/3$ | $\pi/3, \pi, 5\pi/3$ |  |

angular velocity ω_1 during exposure, θ_r and ϕ can be replaced by θ_{r0} (constant) and $\omega_1 t$, respectively. By squaring and adding (3) and (4), (6) is achieved.

$$x^2 + y^2 = (z \tan \theta_{r0})^2. \quad (6)$$

Equation (6) represents a circle with a radius of $z \tan \theta_{r0}$ in a plane parallel to the x-y plane, where z can be arbitrary. The resultant 3-D structure is a “horn” shape. The simulation result is shown in Fig. 16(a) and the corresponding fabricated structure in Fig. 16(b). The horn has a height of $400 \mu\text{m}$ and has been produced from a circular mask window of diameter $50 \mu\text{m}$ and an incidence angle of 50° . The resultant latitudinal angle θ_{r0} is approximately 27° . As can be seen, the simulation matches well the fabricated structure. A broadened bottom is observed due to overexposure. Fig. 16(c), (d) show a multishelled horn from a circular mask window of diameter $30 \mu\text{m}$ fabricated with multiple discrete incidence angles of 0° , 30° , and 55° . The height of the structure is $150 \mu\text{m}$.

A further extension of this technique is to utilize a dynamically driven stage in which both latitudinal and longitudinal angle can be varied during reverse-side exposure through a circular mask window. Consider the case of a periodic variation of the latitudinal angle with a periodic frequency ω_2 and amplitude θ_{r0} occurring simultaneously with continuous rotation in

the longitudinal angle with an angular velocity ω_1 (e.g., $\theta_r = \theta_{r0} \cos \omega_2 t$, $\phi = \omega_1 t$)

$$\begin{aligned} x &= z \tan(\theta_{r0} \cos \omega_2 t) \cos \omega_1 t \\ y &= z \tan(\theta_{r0} \cos \omega_2 t) \sin \omega_1 t \\ z &= z \\ \therefore x^2 + y^2 &= (z \tan(\theta_{r0} \cos \omega_2 t))^2. \end{aligned} \quad (7)$$

Table II shows several examples of the geometries that can be achieved in the case when the latitudinal angle variation is synchronized with the longitudinal rotation. Referring to Table II, the first column shows the frequency of the latitudinal angle variation. The remaining columns describe the resultant structure. The second column gives the distance between the z axis (i.e., the central axis of the mask window) and the exposure pattern at the plane of the resist thickness h . The third column gives the projected 2-D shape of the final 3-D pattern; this shape has peaks and nulls as a function of longitudinal angle which are given in columns 4 and 5. Column 6 shows a 3-D rendering of the final shape as calculated from (7).

The first row of Table II describes a tilting frequency of zero. This indicates static latitudinal angle, which corresponds to the case of Fig. 16(a), (b). The remaining rows of Table II describe the structures achievable by utilizing tilting frequencies which are various fractions or multiples of the longitudinal angular velocity. Very complex structures are potentially achievable with

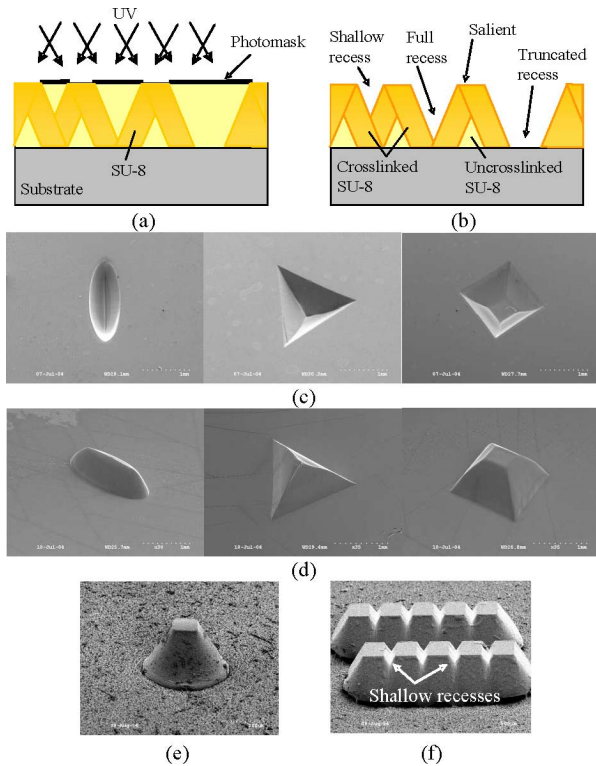


Fig. 17. Continuously rotational inclined UV exposure with various mask patterns. (a) Inclined UV exposure using various patterns in different sizes. (b) Recess patterns with different depth. (c) Resultant recess patterns from a ellipse, a triangle, and a square (from left). (d) PDMS molds copied from the recess patterns (convex lens in half size, tetrahedron, and trapezoidal hexahedron from left). (e) Salient structure from a single clear window. (f) Salient structures from a clear window array.

such a synchronized exposure scheme. It should also be noted that nonsynchronized exposures in conjunction with control of optical dose are also possible, leading to additional possibilities for this technique.

It is also possible to use noncircular mask patterns in conjunction with continuous rotation exposure. The resultant 3-D shape is not only dependent on its geometrical 2-D shape on the photomask but also its inclined angle and slab thickness. Given an inclined angle and a slab thickness, dark and clear mask patterns produce recessed and salient patterns, respectively, as shown in Fig. 17(a), (b). Note that differently sized dark mask patterns result in variation of recess depth: a narrow pattern resulting in a shallow recess shape and a wide one resulting in a full or truncated recess. Fig. 17(c) shows fabricated recess patterns out of an SU-8 slab with a thickness of 1 mm and an incident angle of 45° for three geometrical patterns: a narrow ellipse (a short axis of 0.8 mm and a long axis of 2 mm), a triangle (a side length of 2 mm), and a square (a side length of 1.6 mm). In order to examine the 3-D recess shape, polydimethylsiloxane (PDMS) is cast and separated as shown in Fig. 17(d). All of the resultant patterns show a gradual height change with their varying width in 2-D shape, resulting in a partial 3-D convex lens, a tetrahedron, and a trapezoidal hexahedron (or truncated pyramid) for the ellipse, the triangle, and the square, respectively. In other words, the height and the shape of the 3-D structures are determined by optics for narrow patterns and by both optics and the slab thickness for wide patterns. An inclined angle is also

another variable for the resultant 3-D shape. Fig. 17(e) shows fabricated 3-D structures from clear mask patterns in a dark field photomask. A single clear window gives a salient structure with a gradually varying side wall, which must have contained uncrosslinked SU-8 in it. The uncrosslinked SU-8 can be crosslinked by additional postexposure and postexposure-bake if desired. A clear window array produces at large a salient 3-D structure with shallow recesses resulting from the dark space between the clear patterns as shown in Fig. 17(f).

IV. CONCLUSION

The use of multidirectional UV-exposure techniques has been described. Two categories are discussed: reverse-side exposure through UV-transparent substrates and inclined exposure. The reverse-side exposure scheme has been exploited 1) to achieve high-aspect-ratio polymer structures with SU-8; 2) to fabricate narrowly spaced thick electrodes by using a self-aligned repeatable lift-off process; and 3) to produce tapered structures by means of modified substrates and resultant substrate optics. Inclined exposure has been applied to fabricate 1) inclined solid columns and hollow columns by single inclined exposure; 2) vertical screen filters and complex structures by discrete multidirectional exposure; and 3) various recess and salient structures using inclined rotational exposure. Additional 3-D structures with complementary features can be produced by subsequent molding steps. The demonstrated technique and structures have applications in the areas of RF, optical, microfluidics, and bio, either directly as-fabricated or with additional steps such as micromolding or appropriate metallization. Further, dynamic mode operation has been discussed and some example patterns have been described. Inclined exposure combined with a computer controlled or automation system is expected to have a large impact on the fabrication of complex 3-D structure fabrication.

ACKNOWLEDGMENT

The authors thank Dr. G. Yuan for the fabrication of the rotational stage. They also thank Dr. F. Cros, Dr. Y.-H. Joung, Dr. J.-W. Park, S.-O Choi, and X. Wu for their valuable technical discussion. The fabrication is performed in the Microelectronics Research Center (MiRC) cleanroom in the Georgia Institute of Technology, Atlanta.

REFERENCES

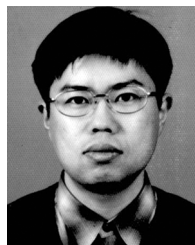
- [1] W. Ehrfeld, F. Gotz, D. Munchmeyer, W. Schelb, and D. Schmidt, "LIGA process: Sensor construction techniques via X-ray lithography," in *Proc. Solid-State Sens. Actuator Workshop*, Hilton Head Island, SC, 1988, pp. 1-4.
- [2] P. Bley, J. Gottert, M. Harmening, M. Himmelhaus, W. Menz, J. Mohr, C. Muller, and U. Wallrabe, "The LIGA process for the fabrication of micromechanical and microoptical components," in *Micro System Technologies*, Berlin, Germany, 1991, pp. 302-314.
- [3] G. P. Behrmann and M. T. Duignan, "Excimer laser micromachining for rapid fabrication of diffractive optical elements," *Appl. Opt.*, vol. 36, pp. 4666-4676, 1997.
- [4] H. Lorenz, M. Despont, N. Fahrni, N. LaBianca, P. Renaud, and P. Vettiger, "SU-8: A low-cost negative resist for MEMS," *J. Micromech. Microeng.*, vol. 7, pp. 121-124, 1997.
- [5] M. Despont, H. Lorenz, N. Fahrni, J. Brugger, P. Renaud, and P. Vettiger, "High-aspect-ratio ultrathick, negative-tone near-UV photoresist for MEMS applications," in *Proc. IEEE Microelectromech. Syst.*, 1997, pp. 518-522.

- [6] F. Cros and M. G. Allen, "High aspect ratio structures achieved by sacrificial conformal coating," in *Proc. Solid-State Sensor and Actuator Workshop*, Hilton Head Island, SC, 1998, pp. 261–264.
- [7] J. Zhang, K. L. Tan, G. D. Hong, L. J. Yang, and H. Q. Gong, "Polymerization optimization of SU-8 photoresist and its applications in microfluidic systems and MEMS," *J. Micromech. Microeng.*, vol. 11, pp. 20–26, 2001.
- [8] Y.-K. Yoon, J. S. Kenney, A. T. Hunt, and M. G. Allen, "Low-loss microelectrodes fabricated using reverse-side exposure for tunable ferroelectric capacitor," *J. Micromech. Microeng.*, vol. 16, pp. 225–234, 2006.
- [9] M. C. Peterman, P. Muie, B. M. Bloom, and H. A. Fishman, "Building thick photoresist structures from the bottom up," *J. Micromech. Microeng.*, vol. 13, pp. 380–382, 2003.
- [10] K. Kim, D. S. Park, H. M. Lu, W. Che, K. Kim, J.-B. Lee, and C. H. Ahn, "A tapered hollow metallic microneedle array using backside exposure of SU-8," *J. Micromech. Microeng.*, vol. 14, pp. 597–603, 2004.
- [11] W. Ehrfeld and A. Schmidt, "Recent developments in deep X-ray lithography," *J. Vacuum Sci. Technol.*, vol. B16, pp. 3526–3534, 1998.
- [12] O. Tabata, K. Terasoma, N. Agawa, and K. Yamamoto, "Moving mask LIGA (M²LIGA) process for control of side wall inclination," in *Proc. IEEE Microelectromech. Syst. (MEMS)*, 1999, pp. 252–256.
- [13] C. Beuret, G.-A. Racine, J. Bobet, R. Luthier, and N. F. de Rooij, "Microfabrication of 3D multidirectional inclined structures by UV lithography and electroplating," in *Proc. IEEE Microelectromech. Syst. (MEMS)*, 1994, pp. 81–85.
- [14] Y.-K. Yoon, J.-H. Park, F. Cros, and M. G. Allen, "Integrated vertical screen microfilter system using inclined SU-8 structures," in *Proc. IEEE Microelectromech. Syst. MEMS*, Kyoto, Japan, 2003, pp. 227–230.
- [15] Y.-K. Yoon, R. Powers, Y. Choi, C. Christophe, and M. G. Allen, "Micromachined polymeric microvasculatures: A three-dimensional microfluidic system using inclined SU-8 structures and laser machining," in *Proc. 226th Amer. Chem. Soc. Nat. Meet., Polymer Division*, New York, 2003.
- [16] M. Han, W. Lee, S.-K. Lee, and S. S. Lee, "Fabrication of 3D microstructures with inclined/rotated UV lithography," in *Proc. IEEE Microelectromech. Syst. (MEMS)*, Kyoto, Japan, 2003, pp. 554–557.
- [17] —, "3D microfabrication with inclined/rotated UV lithography," *Sens. Actuators A*, vol. 111, pp. 14–20, 2004.
- [18] H. Sato, T. Kakinuma, J. S. Go, and S. Shoji, "A novel fabrication of in-channel 3-D micromesh structure using maskless multi-angle exposure and its microfilter application," in *Proc. IEEE Microelectromech. Syst. (MEMS)*, Kyoto, Japan, 2003, pp. 223–226.
- [19] H. Sato, Y. Houshi, and S. Shoji, "Three-dimensional micro-structures consisting of high aspect ratio inclined micro-pillars fabricated by simple photolithography," *Microsyst. Technol.*, vol. 10, pp. 440–443, 2004.
- [20] H. Sato, S. Ito, K. Tajima, N. Orimoto, and S. Shoji, "Functional 3-D PDMS microchannels having slanted grooves embedded walls realizing spiral flow," in *Proc. IEEE Microelectromech. Syst. (MEMS)*, Maastricht, The Netherlands, 2004, pp. 693–696.
- [21] G. Yuan, X. Wu, Y.-K. Yoon, and M. G. Allen, "Kinematically stabilized microbubble actuator arrays," in *Proc. IEEE Microelectromech. Syst. (MEMS)*, Miami, FL, 2005, pp. 411–414.
- [22] R. Yang, J. D. Williams, and W. Wang, "A rapid micro-mixer/reactor based on arrays of spatially impinging micro-jets," *J. Micromech. Microeng.*, vol. 14, pp. 1345–1351, 2004.
- [23] F.-G. Tseng and H.-T. Hu, "A novel micro optical system employing inclined polymer mirrors and fresnel lens for monolithic integration of optical disk pickup heads," in *Proc. 12th Int. Conf. Solid State Sens., Actuators, and Microsystems (Transducers '03)*, Boston, MA, 2003, pp. 599–602.
- [24] K.-Y. Hung, H.-T. Hu, and F.-G. Tseng, "A novel fabrication technology for smooth 3D inclined polymer microstructures with adjustable angles," in *Proc. 12th Int. Conf. Solid State Sens., Actuators, Microsystems (Transducers '03)*, Boston, MA, 2003, pp. 821–824.
- [25] J.-H. Park, Y.-K. Yoon, M. R. Prausnitz, and M. G. Allen, "High-aspect-ratio tapered structures using an integrated lens technique," in *Proc. IEEE Microelectromech. Syst. (MEMS)*, Maastricht, The Netherlands, 2004, pp. 383–386.
- [26] S. Arscott, F. Garet, P. Mounaix, L. Duvillaret, J.-L. Coutaz, and D. Lippens, "Terahertz time-domain spectroscopy of films fabricated from SU-8," *Electron. Lett.*, vol. 35, pp. 243–244, 1999.
- [27] Y.-K. Yoon, J.-W. Park, and M. G. Allen, "Polymer-core conductor approaches for RF MEMS," *J. Microelectromech. Syst.*, vol. 14, no. 5, pp. 886–894, Oct. 2005.
- [28] —, "RF MEMS based on epoxy-core conductors," in *Proc. Solid-State Sens., Actuator, Microsyst. Workshop*, Hilton Head Island, SC, 2002, pp. 374–375.
- [29] Y. Choi, R. Powers, Y.-K. Yoon, and M. G. Allen, "A three-dimensional microfluidic network for cellular perfusion," in *Proc. 7th Int. Conf. Miniaturized Chem. Biochem. Analysis Syst.*, Squaw Valley, CA, 2003, pp. 1001–1004.
- [30] Y.-K. Yoon, B. Pan, P. Kirby, J. Papapolymerou, M. Tentzeris, and M. G. Allen, "Surface micromachined electromagnetically radiating RF MEMS," in *Proc. Solid-State Sens., Actuator, and Microsyst. Workshop*, Hilton Head Island, SC, Jun. 6–10, 2004, pp. 328–331.
- [31] Y.-K. Yoon, B. Pan, J. Papapolymerou, M. M. Tentzeris, and M. G. Allen, "A vertical W-band surface micromachined Yagi-Uda antenna," in *Proc. IEEE AP-S Int. Symp. USNC/URSI Nat. Radio Sci. Meet.*, Washington, DC, Jul. 3–8, 2005.
- [32] Y.-K. Yoon, B. Pan, M. M. Tentzeris, J. Papapolymerou, and M. G. Allen, "Surface-micromachined millimeter-wave antennas," in *Proc. Int. Conf. Solid-State Sens., Actuators, and Microsyst. (Transducers '05)*, Seoul, Korea, Jun. 5–9, 2005, pp. 1986–1989.



Yong-Kyu Yoon (M'04) received the B.S. and M.S. degrees in electrical engineering in 1992 and 1994, respectively, from Seoul National University, Korea. He received the M.S.E.E. degree from the New Jersey Institute of Technology and the Ph.D. degree in electrical and computer engineering from the Georgia Institute of Technology, Atlanta, in 1999 and 2004, respectively.

After graduation, he worked as a Postdoctoral Fellow at the Georgia Institute of Technology. In 2006, he joined the State University of New York (SUNY) at Buffalo as an Assistant Professor in the Electrical Engineering Department. He is interested in the research of development of 3-D MEMS technology; bio/microfluidic systems for the lab-on-a-chip; nanofabrication and its bio/chemical applications; RF passive components and millimeter-wave antennas; microsensors and actuators; electronic and MEMS packaging; and ferroelectric material study and its RF/optical applications.



Jung-Hwan Park was born in Seoul, Korea. He received the B.S. degree in chemical engineering in 1990 from the HanYang University, Korea, and the M.S. degree in chemical engineering in 1992 from the Korea Advanced Institute of Science and Technology (KAIST). He received the Ph.D. degree in biomedical engineering from the Georgia Institute of Technology, Atlanta, in 2004.

From 1992 to 1997, he was with LG Chemical Company as a research scientist. He is currently a Postdoctoral Fellow with the Microelectronics Research Center, Georgia Institute of Technology. His current research interests include 3-D polymeric microstructure fabrication technology, bio/microfluidic systems for the lab-on-a-chip, biocompatible material and its microsystem application, and microsystem for transdermal drug delivery.



Mark G. Allen (M'89–SM'04) received the B.A. degree in chemistry, the B.S.E. degree in chemical engineering, and the B.S.E. degree in electrical engineering from the University of Pennsylvania, Philadelphia, in 1984, 1984, and 1988, respectively, and the S.M. and Ph.D. degrees from the Massachusetts Institute of Technology, Cambridge, in 1989.

He joined the faculty of the Georgia Institute of Technology, Atlanta, in 1989, where he currently holds the rank of a Professor and the J. M. Pettit Professorship in Microelectronics. His research interests are in the areas of micromachining and MEMS, in particular the development and application of new fabrication technologies for micromachined devices and systems.

Prof. Allen was General Cochair of the 1996 IEEE MEMS Conference, and is North American Editor of the *Journal of Micromechanics and Microengineering*.